ACS OMEGA

Open Access

http://pubs.acs.org/journal/acsodf

Article

Quantification of Interactions between Small Molecules and RNA Probes Representative of Myotonic Dystrophy Type 1 Using Affinity Capillary Electrophoresis and UPLC-UV

Mathieu Leveque, Mathilde Wells, Delphine Beukens, Victor Lefebvre, Stéphanie Hambye, and Bertrand Blankert*

Cite This: *ACS Omega* 2025, 10, 62205−62215

Read Online

ACCESS | Metrics & More | Article Recommendations | Supporting Information

ABSTRACT: Myotonic dystrophy type 1 (OMIM #160900) is a multisystemic, autosomal, and dominantly inherited pathology. It is characterized by an expansion (>50) of trinucleotides $[CTG]_n$ on the 3′ untranslated region of the dystrophia myotonica protein kinase gene, transcribed into RNA $[CUG]_n$, aggregating in the nucleus as *foci*. The most accepted pathological mechanism considers the sequestration and dysregulation of proteins, including splicing factors (muscle-blind-like splicing regulator 1 and CUG-binding protein 1) by pathological RNA. Different therapeutic strategies to overcome this defect exist, such as the use of small molecules targeting the pathological RNA to prevent sequestration. Among these small molecules, pentamidine (PTMD), an antiprotozoal drug, has previously been shown to interact with a $[CUG]_n$ repeat. In this context, we developed a fine-tuned affinity capillary electrophoresis (ACE) method that provides highly repeatable migration times. This is a crucial point, as all subsequent calculations for apparent affinity constant (Ka_{app}) determination rely on them. Afterward, we quantified the interactions between pentamidine and two RNA probes: $[CUG]_{95}$, representative of the disease, and $[CUG]_{14}$ as a negative control. The results indicated an excellent affinity between $[CUG]_{95}$ and PTMD. Selectivity was assessed by comparing the Ka_{app} values: $(6.1 \pm 0.4) \times 10^3$ M^{-1} and $(3.8 \pm 0.3) \times 10^3$ M^{-1} for the positive and negative controls, respectively. For the first time, an orthogonal UPLC-UV methodology was applied to corroborate the ACE results. No significant differences were observed between the two analytical methods. To overcome the documented toxicity related to pentamidine, different libraries of small molecules have been investigated by the ACE method. Among these, two compounds, neomycin and chloroquine, demonstrated interactions with the pathological RNA model. Therefore, their affinities toward the positive and negative controls were quantified to assess the selectivity of these potential therapeutic candidates.

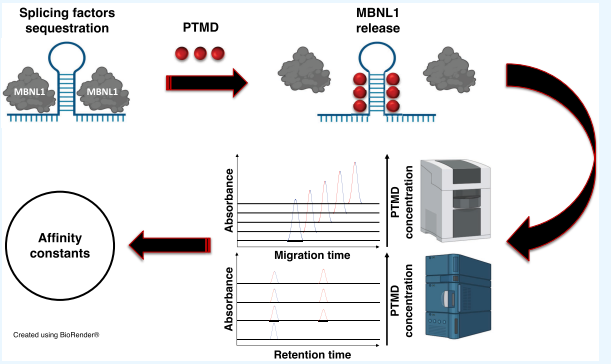

INTRODUCTION

Myotonic dystrophy type 1 (DM1), also known as Steinert's disease, is an autosomal-dominant inherited pathology belonging to the noncoding expansion disorders, including myotonic dystrophy type 2 (DM2), fragile X-associated tremor/ataxia syndrome (FXTAS), Huntington disease-like 2 (HDL-2), and some spinocerebellar ataxia (SCA) as well.[1] DM1 was first described by Hans Steinert in 1909 and was characterized in 1992 as a trinucleotide $[CTG]_n$ expansion (>50) located on the 3′ untranslated region (3′ UTR) of a gene coding for a protein kinase (DMPK: dystrophia myotonia protein kinase) located on chromosome 19 (19q13.3).[2−4] The transcription of that DNA mutation results in RNA $[CUG]_n$ expansions folding into stable hairpin structures.[5] Even though different pathological mechanisms have been described, the most accepted one is an RNA gain-of-function, which involves these structures aggregating in RNA *foci* in the nucleus, leading to the sequestration of different proteins.[6−8] Based on this, two major pathological consequences have emerged: *(i)* the direct interaction of $[CUG]_n$ and the muscle-blind-like splicing regulator 1 (MBNL1) inducing its sequestration and down-regulation,[9−11] and *(ii)* the indirect effect of RNA expansions on the CUG-binding protein 1 (CUG-BP1), leading to its upregulation due to the stabilization of the protein kinase C (PKC) or its downregulation due to the stabilization of the glycogen synthase kinase 3β (GSK3β).[12 −14] As MBNL1 and CUG-BP1 regulate the alternative splicing of mRNA, their dysregulation disrupts the splicing of RNA targets, resulting in

Received: September 21, 2025
Revised: October 24, 2025
Accepted: October 30, 2025
Published: December 7, 2025

truncated proteins (alternative splicing defects in DM1 were reviewed by López-Martinez et al.[15]). This results in a multisystemic disease affecting almost all systems such as muscles with dystrophy and myotonia, the heart with conduction defects, eyes with cataracts, cognitive and endocrine systems with diabetes among others.[16] Based on a meta-analysis, the prevalence of DM1 was estimated to be around 9.27 cases per 100,000.[17] However, this value is likely underestimated since a recent study based on a genetic diagnosis in the state of New York showed a prevalence of 47.6 cases per 100,000 births.[18] Even though no curative treatments for DM1 are available, several therapeutic strategies have been hypothesized. These include the inhibition of transcription, degradation of RNA expansions, upregulation or down-regulation of MBNL1 and CUG-BP1, gene therapy, and suppression of the interactions between proteins and RNA expansions using either antisense oligonucleotides or small molecules.[19,20] Currently, there is a growing interest in the use of small molecules in the context of DM1 because of their high biodistribution and the availability of clinical data on repurposed drugs. Warf et al. were the first to demonstrate that small molecules were capable of disrupting the complex formed between sequestered proteins and RNA hairpin structures.[21] The study focused on pentamidine (PTMD), an antiprotozoal drug currently used for the treatment of *Pneumocystis carinii* and *Trypanosoma gambiense* infections (Figure 1). An electromobility shift assay (EMSA) showed that

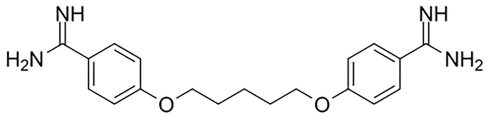

Figure 1. Structure of pentamidine.

this compound reduced the $[CUG]_4$-MBNL1 complex. Further results demonstrated that PTMD tended to decrease the number of RNA *foci* in the nucleus *in vitro*. Moreover, PTMD partially restored the alternative splicing of RNA of several genes dysregulated in DM1. *In vitro*, alternative splicing of the RNA of the cardiac muscle troponin T gene (cTNT) and the insulin resistance gene (IR) was indeed rescued in HeLa cells expressing 960 repeats of the trinucleotide [CTG], whereas the voltage-dependent chloride channel gene (Clc-1) and the sarcoplasmic/endoplasmic reticulum calcium ATPase 1 gene (Serca-1) were rescued *in vivo* in mice expressing 250 [CTG] repeats. Even though PTMD displayed interesting results toward the targeted RNA expansions, its toxicity limits its use in the context of DM1, as the concentrations required to obtain a complete rescue of alternative splicing showed high mortality both *in vitro* and in *vivo*.

Several studies have investigated the use of pentamidine analogues in order to maintain or increase their efficiency while decreasing their toxicity.[22−27] To assess the potential of new therapeutic candidates targeting RNA expansions representative of DM1, different methods allowing the quantification of interactions between these two species should be used. As a common output of these assays, the affinity constant (*Ka*) is a numerical value describing the strength of the affinity between two compounds, usually referred to as analytes and ligands (both terms are used arbitrarily and can be inverted), represented in the following equations as A and L, respectively:[28]

$$A + L \underset{k_{off}}{\overset{k_{on}}{\rightleftharpoons}} AL \tag{1}$$

In eq 1, k_{on} is the association rate and k_{off} is the dissociation rate. At equilibrium,

$$k_{on}[A][L] = k_{off}[AL] \tag{2}$$

In eqs 2 and 3, [A], [L], [AL], and K_d are the molar concentrations of the free analyte, free ligand, complex, and dissociation constant, respectively. When steady state is achieved, the affinity constant *K*a is defined by eq 3:

$$K_a = \frac{1}{K_d} = \frac{k_{on}}{k_{off}} = \frac{[AL]}{[A][L]} \tag{3}$$

Several analytical techniques have already been developed to quantify interactions with nucleic acids, such as competition dialysis, ultracentrifugation, gel electrophoresis, capillary electrophoresis, fluorescence intensity, fluorescence anisotropy, UV−visible spectrophotometry, circular dichroism, surface plasmon resonance, biolayer interferometry, isothermal titration calorimetry, microscale thermophoresis, and high-performance liquid chromatography.[29,30] Among them, capillary electrophoresis represents a powerful technique that has been used many times to quantify the affinities between two compounds. Six modes of capillary electrophoresis have been described in the literature to investigate biointeractions. These modes differ either in the composition of the sample and the background electrolyte (running buffer or analyte or a mixture of analyte and ligand) or from the extracted response (peak intensity, peak area, or migration time): capillary zone electrophoresis (CZE), affinity capillary electrophoresis (ACE), frontal analysis (FA), vacancy peak technique (VP), vacancy affinity capillary electrophoresis (VACE) and Hummel-Dreyer technique (HD).[31] ACE was first described in 1992 by Chu et al. for the quantification of affinities between a protein and ligands.[32] ACE measurements are based on an electrophoretic mobility shift when interactions occur relative to a change in the charge/mass ratio:

$$\mu_e = \frac{q}{6\pi\eta r} \tag{4}$$

In eq 4, μ_e, q, η, and r correspond to the electrophoretic mobility of the analyte, the charge state, the viscosity of the medium, and the radius of the analyte, respectively.

In ACE, the sample containing the analytes is injected into a capillary filled with a background electrolyte and ligands at concentrations that increase between each run. As the concentrations increased, the dynamic interactions were enhanced, resulting in lower shift values of the analyte electrophoretic mobility, corresponding to higher migration times in the recorded electropherogram. Different mathematical models have been used to quantify the affinity constants of ACE, such as nonlinear regression, *x*-reciprocal, *y*-reciprocal, and double reciprocal.[33,34] Even though all of these fittings can be used in ACE and give similar results, nonlinear regression shows a higher precision and should be considered more:[35,36]

$$\Delta\mu = \frac{\Delta\mu_{max} K_a[L]}{1 + K_a[L]} \tag{5}$$

In eq 5, $\Delta\mu$ is the difference in electrophoretic mobilities between analytes without and with ligands at increasing concentrations, $\Delta\mu_{max}$ is the highest $\Delta\mu$ observed, *K*a is the

https://doi.org/10.1021/acsomega.5c09840
ACS Omega 2025, 10, 62205−62215

affinity constant, and [L] is the ligand concentration. By plotting $\Delta\mu$ as a function of [L], the slope of the nonlinear curve allowed the quantification of *K*a. Since this mathematical model assumes a 1:1 stoichiometry, the determined affinity constant for other stoichiometries corresponds to the apparent affinity constant (Ka_{app}), which represents the global affinity of a ligand to an analyte.[37]

Even though ACE has been carried out several times to study biointeractions, there are only around 20 scientific articles retrieved in Scopus regarding the quantification of affinity constants between the nucleic acids and ligands. Among them, our team has previously confirmed the interaction of PTMD with a $[CUG]_{50}$ probe by ACE and highlighted neomycin, an aminoglycoside antibiotic, as a binding partner of that RNA probe.[26]

The potential therapeutic role of small molecules targeting RNA expansions in the context of DM1 has been demonstrated. The present research work aimed to standardize and strongly consolidate the affinity capillary electrophoresis method using PTMD as a reference molecule. As mentioned by Nowak et al., the Achilles' heel of capillary electrophoresis experiments is the poor repeatability of the results, including migration times (MT).[38] This parameter is a key player in the context of ACE. All subsequent calculations for Ka_{app} determination will be based on this fundamental factor. Highly repeatable MT is required to calculate reliable electrophoretic mobilities and, therefore, reliable apparent affinity constants. Only a very few scientific papers have evoked the crucial role of MT and investigated the repeatability of MT in the field of affinity capillary electrophoresis using nucleic acids as analytes. In light of this, we aim to bring to the scientific community a tailored ACE method capable of generating results with a very high degree of repeatability. Parallelly, two synthesized RNA probes ($[CUG]_{95}$ and $[CUG]_{14}$), representative of pathological and nonpathological states, were utilized.

To further confirm the reliability of the approach, the results obtained by ACE were compared with those obtained by using an orthogonal UPLC-UV method. Finally, different libraries of organic molecules were tested by ACE to identify potential therapeutic candidates for DM1. Among them, chloroquine has emerged as a promising compound that requires further evaluation.

MATERIALS AND METHODS

Reagents

Ampicillin (Alfa Aesar), H-PTFE 0.2 μm syringe filters (Whatman), and ethanol 96% (J.T. Baker) were purchased from VWR. LB broth, DEPC, HEPES and HEPES molecular biology grade, EDTA of molecular biology grade, MOPS, formaldehyde of molecular biology grade, pentamidine isethionate, chloroquine diphosphate, neomycin sulfate, and poly(ethylene oxide) 200k were bought from Merck. Kits from ZymoResearch, including ZymoPure II Plasmid Gigaprep and DNA Clean and Concentrator, were obtained from Baseclear. The restriction enzyme *Hin*dIII and associated buffer, Riboruller low range RNA ladder, including the loading dye, were purchased from Fisher Scientific. NaOH, $CH_3COOH.3H_2O$, HCl, and dimethyl sulfoxide (DMSO) were purchased from ChemLab. HiScribe SP6 *in vitro* transcription kit (NEB), agarose molecular biology grade, and silica capillaries (Polymicro) were obtained from Bioke, Eurogentec, and Mouser Electronics, respectively. Acetonitrile (ACN) of UPLC-grade was provided by BioSolve. The other compounds analyzed in this study (Tables S-1 and S-2, Supporting Information) were purchased from Certa, Fagron, Merck, ThermoFisher, ABC Chemicals, Pharma Chemicals, FSA Chemicals, and Alpha Aesar. All solutions were prepared using ultrapure deionized water with a resistivity of 18.2 MΩ.cm.

RNA Probe Synthesis

RNA probes ($[CUG]_{95}$ and $[CUG]_{14}$) were synthesized in-house. Plasmids pSP72 (provided by Dr. Denis Furling, Institute of Myology, Paris, France) were previously inserted into competent *Escherichia coli* and stored in a glycerol stock at −80 °C. Bacteria were cultured in LB broth (20 g/L) containing ampicillin (100 μg/mL) and centrifuged. Plasmids were then extracted using a ZymoPure II Plasmid Gigaprep kit, linearized by the restriction enzyme *Hin*dIII, and purified using a DNA Clean and Concentrator-25 kit based on the solid-phase extraction process. *In vitro* transcription was performed with a HiScribe SP6 *in vitro* transcription kit. The resulting RNA was purified using LiCl precipitation and finally reconstituted in HEPES (5 mM, pH 7.4) to reach 100 μg/mL (the quantification of RNA was performed by measuring the absorbance at 260 nm), corresponding to 1.03 and 5.16 μM of $[CUG]_{95}$ and $[CUG]_{14}$, respectively. To evaluate the quality of RNA probes, defined as RNA lengths, gel slab electrophoresis under denaturing conditions was performed using a 2% agarose gel (made with 9 mL of 37% formaldehyde, 5 mL of MOPS 10×, and 36 mL of RNase-free water) and MOPS 1× as the running buffer. A voltage of 50 V was applied, and the migration was finally compared with an RNA ladder (Figure 2).

Affinity Capillary Electrophoresis

Capillary electrophoresis experiments were carried out with an Agilent 7100 CE system managed by using Chemstation B.04.03-SP1 software. The device was equipped with a Diode Array Detector (set at 260 nm). The samples were injected

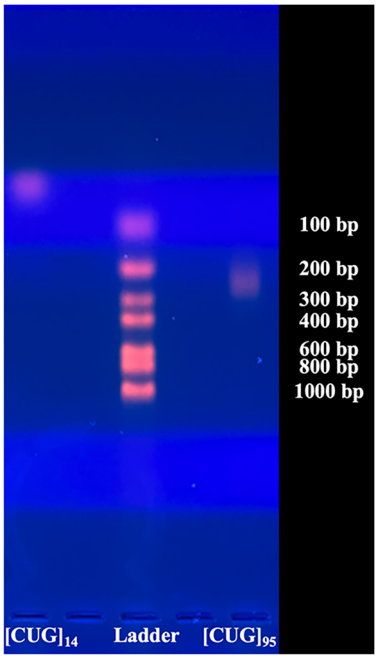

Figure 2. Gel electrophoresis of $[CUG]_{14}$ and $[CUG]_{95}$.

https://doi.org/10.1021/acsomega.5c09840
ACS Omega 2025, 10, 62205−62215

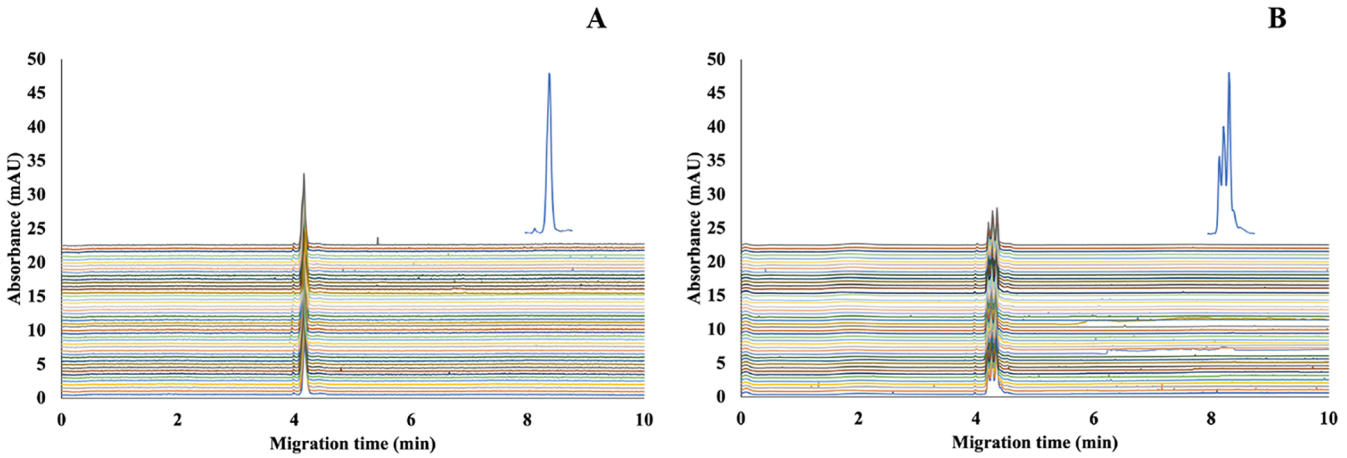

Figure 3. Electropherograms (n = 45) of (A) $[CUG]_{95}$ and (B) $[CUG]_{14}$. The peak shapes are represented in the upper right corner of the electropherograms.

hydrodynamically (50 mbar × 5 s), and a negative voltage of −15 kV was applied at the inlet using platinum electrodes. The bare fused silica capillary had an internal diameter (ID) of 50 μm, an outer diameter (OD) of 365 μm, a total length (L_t) of 40 cm, an effective length (L_e) of 31.5 cm, and was kept at 25 °C. The capillary was coated using a PEO dynamic coating process, allowing the migration of negatively charged RNA toward the detection area located close to the anode. The coating protocol was an optimized version of previously reported ones.[26,39−43] The PEO stock solution (1.1111% w/v) was prepared by adding 0.2222 g of PEO 200k in 20.0 mL of ultrapure water heated at 50 °C in a 50 mL conical flask and handshaked vigorously for 5 min. The PEO working solution was made by adding 9 parts of the stock solution and 1 part of HCl 250 mM, and vortexing for 15 s. The first coating of a new capillary was done by flushing water, 1 M NaOH, 0.1 M NaOH for 5 min each, water for 20 min, PEO 1% in HCl 25 mM for 5 min, and the background electrolyte (BGE) for 3 min. Each day, the coating was regenerated by flushing water for 3 min, PEO 1% for 5 min, and BGE for 3 min. The coating was also performed before each injection by passing through capillary water for 3 min, PEO 1% for 5 min, and finally BGE for 3 min. The BGE was either 50 mM HEPES, pH 7.4, or 50 mM HEPES, pH 7.4, containing 1% (v/v) DMSO for repeatability studies, while it contained ligands at different concentrations for ACE analysis. The concentrations of both $[CUG]_{95}$ and $[CUG]_{14}$ were constant at 1.03 and 5.16 μM, respectively. All solutions used in the capillary electrophoresis experiments were filtered through 0.2 μm H-PTFE syringe filters, except for the RNA samples and PEO solutions. BGE solutions were also sonicated for 15 min before use.

UPLC-UV

An Acquity H-Class UPLC system (Waters), equipped with a quaternary solvent manager, a column manager containing an HSS T3 C18 1.8 μm 2.1 × 100 mm column, a flow-through needle as a sample manager, and a Photodiode Array Detector, was used to perform the experiments. The device was controlled by using Empower 3. The samples and the column were maintained at 25 °C, the volume of injection was 10 μL, and the seal wash, preinjection, and postinjection washes were performed using a mixture of 10% acetonitrile. The mobile phase was composed of an aqueous phase (50 mM HEPES, pH 7.4) filtered through a 0.2 μm H-PTFE syringe filter and an organic phase (acetonitrile). The three factors studied by DOE were *(i)* the duration of the isocratic phase (100% aqueous phase) before starting the gradient (A), *(ii)* the gradient duration to reach 100% of the organic phase (B), and (iii) the flow rate of the mobile phase (C). Factors A, B, and C were tested in the ranges 1−2 min, 3−5 min, and 0.1−0.2 mL/min, respectively. In this model, we defined the constraints as follows: the retention time of RNA should be minimized, and the selectivity should be 1.25. All UPLC experiments used RNA $[CUG]_{95}$ or $[CUG]_{14}$ at 0.516 or 2.58 μM, respectively. The mobile phases were sonicated for 20 min before use.

Data Analysis

Linear and nonlinear regressions were performed using GraphPad. Ka_{app} values were expressed as Ka_{app} ± standard error. Standard errors were calculated with GraphPad for ACE experiments and R software for UPLC-UV experiments. Stat-Ease 360 was used as the DOE software for the optimization of the UPLC method, and ANOVA tests were carried out with Excel.

RESULTS AND DISCUSSION

Affinity Capillary Electrophoresis

Capillary Coating Procedure. In capillary electrophoresis (CE), the capillary coating step has two main objectives. First, it minimizes the adsorption of chemical species onto the negatively charged silanol groups on the bare capillary wall, which can cause peak distortion. Second, it stabilizes the electro-osmotic flow (EOF). EOF is a bulk solvent movement driven by the interactions between the positive ions present in the background electrolyte and the negative charges of the silanol groups on the inner capillary surface. Since these positive ions are usually solvated, upon the application of a voltage, they will migrate from the anode to the cathode, creating a solvent flow through the capillary. The EOF value is typically higher than the the electrophoretic mobility of an analyte, and it can hinder the migration of negatively charged compounds, such as RNA, toward the positive electrode, thereby affecting their detection. Therefore, the reduction and the monitoring of this flow are critical for RNA assays using ACE, and capillary coating constitutes a tricky parameter that must be optimized to improve the repeatability of migration times across analyses. In this study, poly(ethylene oxide) (PEO) was used for the capillary coating. To evaluate the

https://doi.org/10.1021/acsomega.5c09840
ACS Omega 2025, 10, 62205−62215

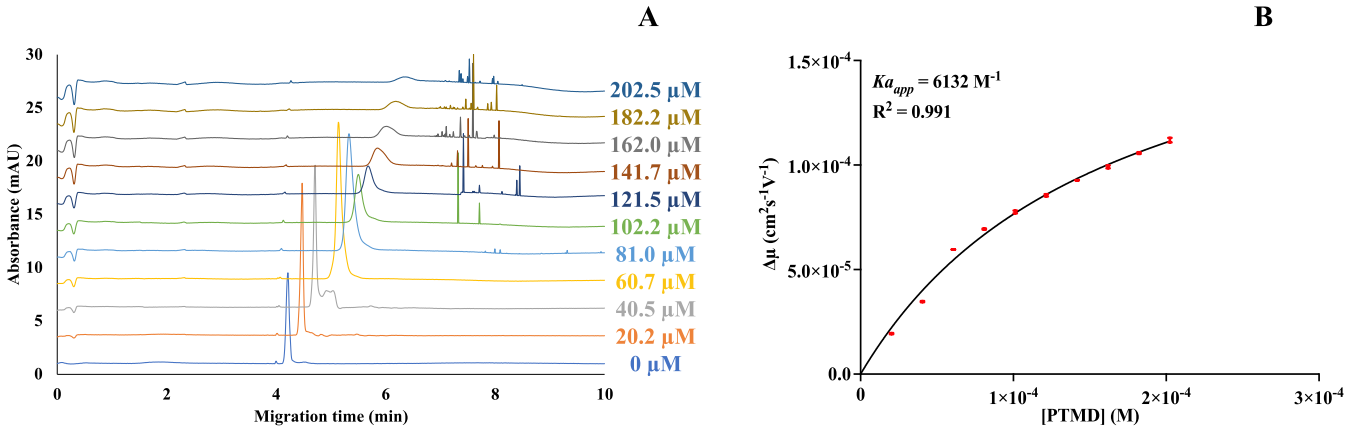

Figure 4. Electropherograms of ACE assays (A) and nonlinear regression for the quantification of the apparent affinity constant (B) between 1.03 μM $[CUG]_{95}$ and PTMD.

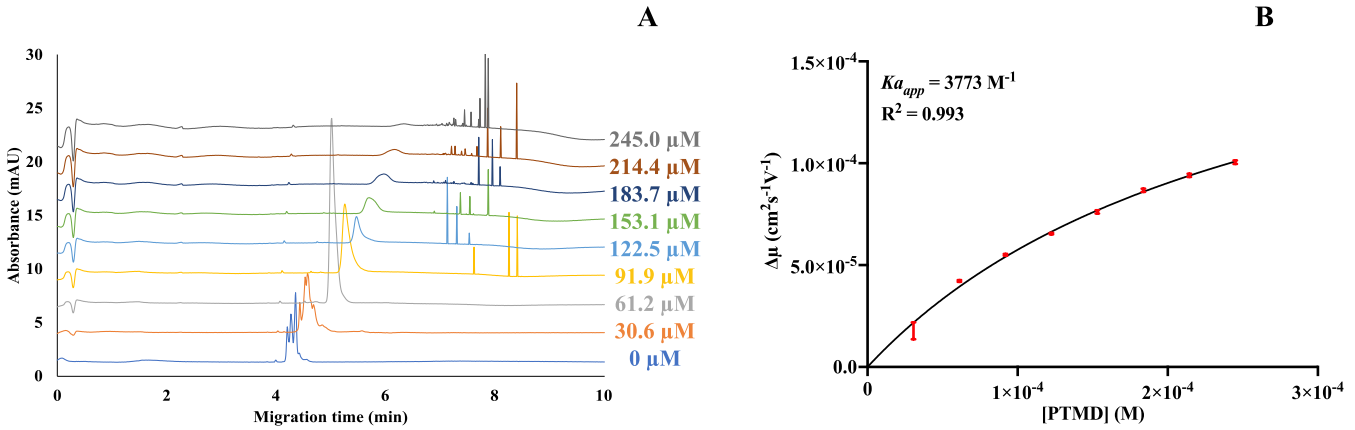

Figure 5. Electropherograms of ACE assays (A) and nonlinear regression for the quantification of the apparent affinity constant (B) between 1.03 μM $[CUG]_{14}$ 5.16 μM and PTMD.

repeatability of migration times, three sequences (n = 3) of 15 injections were performed over 3 consecutive days using either RNA $[CUG]_{95}$ at 1.03 μM (Figure 3A) or $[CUG]_{14}$ (Figure 3B) at 5.16 μM in 5 mM HEPES, pH 7.4, with 50 mM HEPES, pH 7.4, as the background electrolyte. The RSDs (%) of migration times for $[CUG]_{95}$ have been determined intraday at 0.24, 0.28, and 0.23%, and 0.26% interdays. Similar values were obtained for $[CUG]_{14}$ with 0.20, 0.14, and 0.14% intraday and 0.22% interday. To the best of our knowledge, the literature does not mention any threshold value to deem the repeatability of MT acceptable in ACE. Therefore, we defined an RSD of 0.5% for considering the MT as highly repeatable. Based on these values, these results highlight PEO as a suitable coating polymer to manage and reduce EOF during capillary electrophoresis experiments.

The associated electropherograms showed a triple peak when $[CUG]_{14}$ was analyzed by CE (Figure 3B). It was hypothesized that the synthesis of $[CUG]_n$ repeats by *in vitro* transcription led to fragments of different sizes due to RNA polymerase slippage, represented as a Gaussian curve with the maximum corresponding to the desired fragment.[44] This hypothesis was supported by the rather diffuse spots observed on gel electrophoresis (Figure 2). Since capillary electrophoresis is capable of separating small oligonucleotides without the need for sieving matrices, it was assumed that the different peaks observed on the electropherograms of $[CUG]_{14}$ could be due to different fragments with different numbers of base pairs, whereas no separation occurred when analyzing larger RNA such as $[CUG]_{95}$.[45] Even though fragments of different sizes were generated during *in vitro* transcription, it was assumed that their length variation, limited to a few nucleotides, would not significantly influence the measured apparent affinity constants. Therefore, the peak with the highest intensity was monitored for different analyses of $[CUG]_{14}$.

***Ka_{app}* Assessment between $[CUG]_{95}$ and PTMD.** The previously optimized capillary electrophoresis method demonstrated a high degree of repeatability in terms of migration times, supporting the use of ACE as a powerful tool to quantify biomolecular interactions. The apparent affinity constants were determined by injecting a constant concentration of analytes while the capillary was filled with different concentrations of ligands. The migration times were then recorded, and the electrophoretic mobilities were calculated. When interactions occurred, the analyte's charge-to-radius ratio was affected, causing an increase of the migration time due to a reduction in electrophoretic mobility. The apparent affinity constants were calculated using a nonlinear regression, as described in eq 5. By plotting the change in electrophoretic mobility ($\Delta\mu = \mu_0 - \mu_e$) of the analyte as a function of ligand concentration, Ka_{app} was determined from the slope. In this study, RNA $[CUG]_{95}$ at 1.03 μM in 5 mM HEPES, pH 7.4, was used as the analyte, while pentamidine isethionate at concentrations ranging from 0 to 202.5 μM in 50 mM HEPES, pH 7.4, served as the ligand solution (Figure 4A). Each concentration condition was

https://doi.org/10.1021/acsomega.5c09840
ACS Omega 2025, 10, 62205−62215

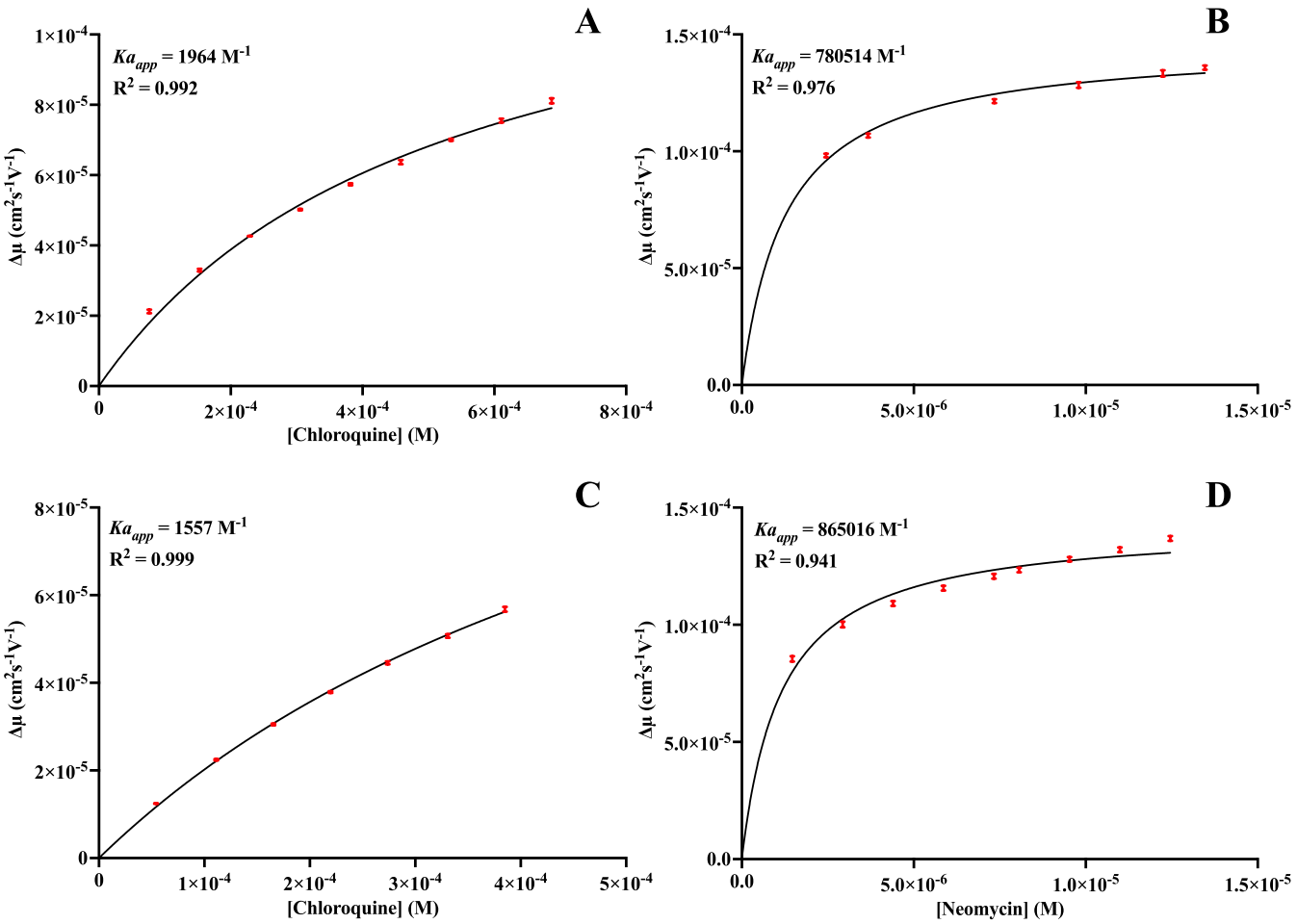

Figure 6. Nonlinear regressions for the quantification of the apparent affinity constants between (A) $[CUG]_{95}$ and chloroquine, (B) $[CUG]_{95}$ and neomycin, (C) $[CUG]_{14}$ and chloroquine, and (D) $[CUG]_{14}$ and neomycin.

carried out in triplicate (n = 3), and the resulting Ka_{app} between the pathological RNA probe and PTMD was (6.1 ± 0.4) × 10^3 M^{-1} (Figure 4B). These results demonstrated that PTMD interacted with the RNA probe $[CUG]_{95}$, representative of DM1.

The associated electropherograms (Figure 4A) showed that the peak's intensity varied when the concentration of PTMD was increased. This phenomenon might be explained by the interaction of PTMD with $[CUG]_{95}$. When the concentration of PTMD was low, a hyperchromic effect was observed due to the denaturation of RNA structures, whereas when the concentration of PTMD was increased, a hypochromic effect appeared related to the stabilization of RNA structures.[46]

PTMD Selectivity Evaluation Using $[CUG]_{14}$. Since the interaction of PTMD with a pathological model of DM1 was quantified with RNA containing 95 repetitions, the selectivity of this compound was evaluated using $[CUG]_{14}$ as a negative control (nonpathologic probe). During this research, a candidate was considered as selective to the pathological model when its Ka_{app} value was higher and significantly different (via ANOVA test) from that measured toward the negative control. The apparent affinity constant was assessed in the same way, as described in the previous paragraph. RNA $[CUG]_{14}$ was prepared in 5 mM HEPES, pH 7.4, at 5.16 μM, and pentamidine was added to the background electrolyte (HEPES 50 mM, pH 7.4) at concentrations ranging from 0 to 245.0 μM (Figure 5A). The quantification of Ka_{app} was performed by testing each concentration in triplicate, exhibiting a value of (3.8 ± 0.3) × 10^3 M^{-1} (Figure 5B). The apparent affinity constant values obtained for the pathological and nonpathological models were compared using an analysis of variance (ANOVA) test. The p-value was around 6 × 10^{-4}, indicating that the difference in Ka_{app} between the two models was significant at a risk α of 5%.

These results emphasized a higher interaction level of PTMD with respect to the pathological model and significantly different Ka_{app} values between the two RNA probes. This suggests that the PTMD structure could serve as an appropriate reference for identifying other candidates capable of releasing sequestered splicing factors in DM1 while reducing toxicity. Moreover, the electropherograms of ACE (Figure 5A) showed that the peak's intensity corresponding to the analyte varied when the ligand concentration increased. This phenomenon might still be the result of conformational changes when interactions occurred, leading to molar absorptivity changes.[26,46]

Evaluation of Aqueous Soluble Molecules. Even though molecules structurally related to PTMD could be of great interest in this context, other chemical entities should also be considered. Therefore, by means of the optimized ACE method, a library of aqueous soluble compounds was studied to highlight potential candidates with affinities toward the pathological RNA probe. Different molecules were dissolved at high concentrations (Table S-1, Supporting Information) in

https://doi.org/10.1021/acsomega.5c09840
ACS Omega 2025, 10, 62205−62215

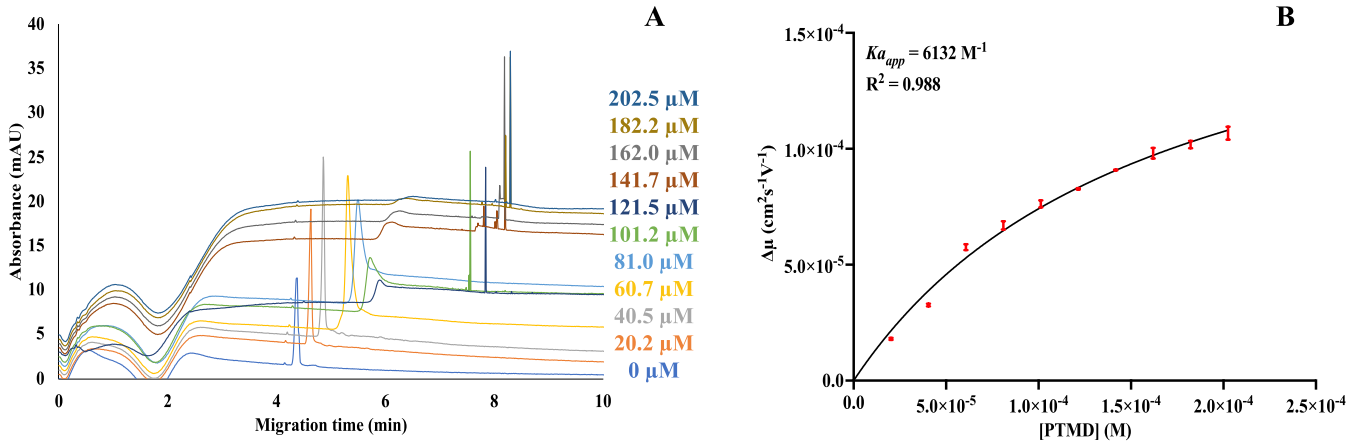

Figure 7. Electropherograms of ACE assays (A) and nonlinear regression for the quantification of the apparent affinity constant (B) between 1.03 μM $[CUG]_{95}$ and PTMD when DMSO is added to the BGE.

the BGE (HEPES 50 mM, pH 7.4) and analyzed by ACE using $[CUG]_{95}$ at 1.03 μM as the analyte. Among the 39 compounds studied, chloroquine and neomycin have been highlighted to interact with the pathological RNA model since the peaks of the analytes disappeared on the electropherograms due to conformational changes (Figure S-1, Supporting Information). Therefore, the interactions of these candidates toward the same RNA probe were measured in triplicate at concentrations ranging from 0−686.9 and 0−13.4 μM for chloroquine and neomycin, respectively. The apparent affinity constants were $(2.0 \pm 0.1) \times 10^3$ M^{-1} for chloroquine and $(7.8 \pm 0.4) \times 10^5$ M^{-1} for neomycin (Figure 6). The selectivity of these compounds was evaluated using the RNA probe $[CUG]_{14}$ at 5.16 μM in the ranges 0−385.0 and 0−12.5 μM for chloroquine and neomycin, respectively. The Ka_{app} values obtained by performing ACE experiments (n = 3) were $(1.56 \pm 0.07) \times 10^3$ M^{-1} for chloroquine and $(8.7 \pm 0.6) \times 10^5$ M^{-1} for neomycin (Figure 6). Since the interaction level of chloroquine was higher toward $[CUG]_{95}$, the apparent affinity constants obtained for both RNA probes were compared using an ANOVA test. The p-values were around 2×10^{-4}, indicating that the difference in Ka_{app} between the two models was significant at a risk α of 5%. Therefore, these results highlight that chloroquine is selective to the pathological model and will require further evaluation, whereas neomycin is not.

Assessment of the Impact of DMSO. Despite chloroquine emerging as a potential candidate in the context of DM1 from the initially considered library composed only of aqueous soluble molecules, a modification of the BGE composition was carried out to enlarge the field of compounds that can be analyzed by ACE. To achieve this objective, 1% DMSO (v/v) was added to the BGE to improve its solubilization properties. This concentration was utilized since it is considered a noncytotoxic one.[47]

A preliminary study was performed using the RNA probe $[CUG]_{95}$ at 1.03 μM to ensure that DMSO did not affect the repeatability of the migration times by analyzing three sequences (n = 3) of 15 injections over 3 days with 50 mM HEPES, pH 7.4, containing 1% (v/v) DMSO as BGE (Figure S-2, Supporting Information). The RSDs (%) of migration times have been calculated intraday at 0.24, 0.13, and 0.19% and 0.23% interdays. Since these RSDs were below the threshold of 0.5%, these results demonstrate that the use of DMSO as cosolvent did not affect the repeatability of the migration times. However, Lee et al. previously reported a modification of the affinity constants measured by spectrofluorimetry between RNA and small molecules when DMSO was added to improve their solubilization.[48] To assess the influence of DMSO on the apparent affinity constant obtained by ACE, the interaction of PTMD with the pathological RNA probe was quantified using 50 mM HEPES, pH 7.4, containing 1% (v/v) DMSO as the BGE. In this study, 1.03 μM $[CUG]_{95}$ was used as the analyte, while pentamidine dissolved in the BGE at concentrations ranging from 0 to 202.5 μM was used as the ligand. The experiments were carried out in triplicate, and the resulting apparent affinity constant was $(6.1 \pm 0.5) \times 10^3$ M^{-1} (Figure 7). The Ka_{app} values obtained with and without DMSO were compared using an ANOVA test (risk α of 5%). The p-value was 0.98, indicating that 1% (v/v) DMSO did not significantly influence the apparent affinity constant calculated by ACE.

Evaluation of Aqueous Insoluble Molecules. Consequently, an aqueous insoluble compound library was investigated to identify new potential candidates. Different ligands were dissolved at high concentrations (Table S-2, Supporting Information) in the BGE supplemented with DMSO, and the analyte was 1.03 μM $[CUG]_{95}$. However, among the 19 molecules analyzed, none of them showed interactions with the pathological model of DM1. Therefore, in the future, other libraries of both aqueous soluble and aqueous insoluble compounds should be evaluated to identify new candidates capable of interacting with pathological RNA probes.

UPLC-UV. In the same context, a UPLC-UV method was developed and optimized by applying a design of experiments process (DOE) to investigate the interactions between PTMD and RNA and compare the results obtained by ACE. UV−visible spectroscopy is another analytical technique commonly used to quantify the interactions between RNA and small molecules. Affinity constants can be extracted by recording the absorbance intensity of an analyte whose concentration is constant while varying that of a ligand.[49−55] However, since the absorbance spectra of RNA and PTMD are overlaid, a separation method was necessary to measure the absorbance variations occurring when PTMD was added at different concentrations to RNA. Several recent research papers

https://doi.org/10.1021/acsomega.5c09840
ACS Omega 2025, 10, 62205−62215

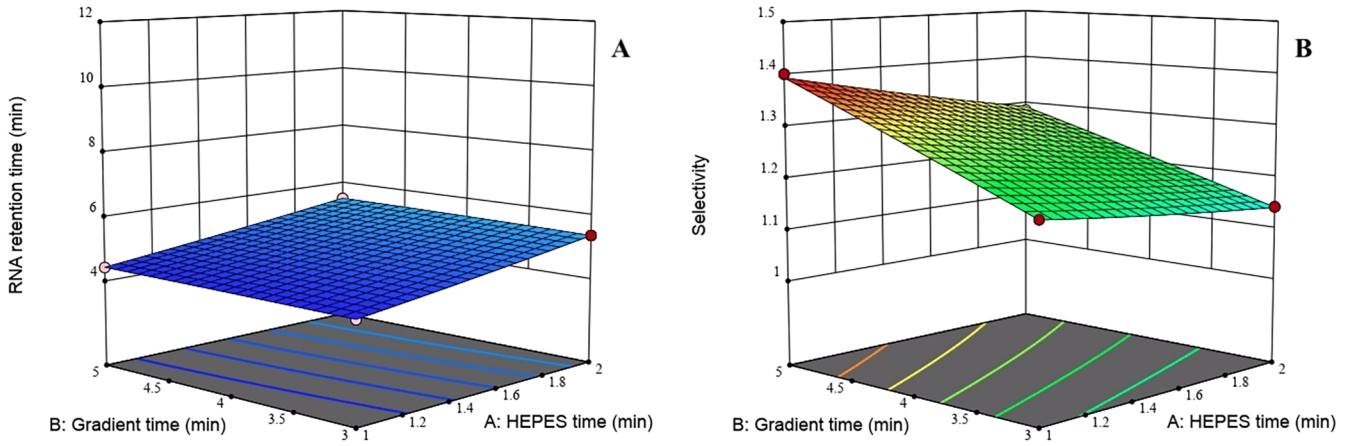

Figure 8. Response surface methodology showing the influence of the duration of the aqueous phase before starting the gradient and the gradient time to reach 100% of the organic phase when the flow was 0.2 mL/min on the (A) retention time of RNA and (B) selectivity between RNA and PTMD.

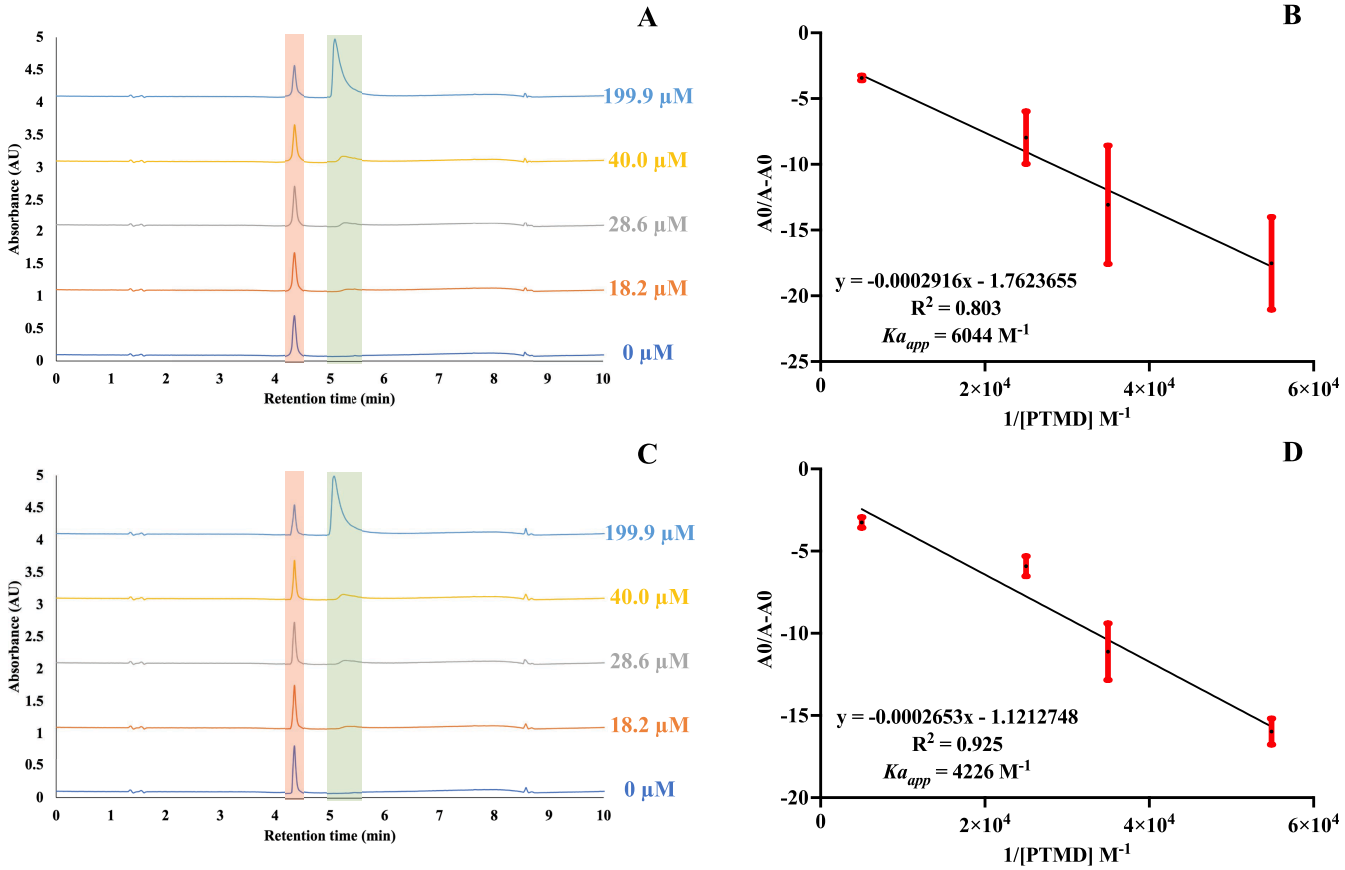

Figure 9. Chromatogram of UPLC-UV assays (A) and double reciprocal for the quantification of the apparent affinity constant (B) between 1.03 μM $[CUG]_{95}$ and PTMD. The chromatogram of UPLC-UV assays (C) and double reciprocal for the quantification of the apparent affinity constant (D) between 5.16 μM $[CUG]_{14}$ and PTMD. The peaks highlighted in red and green correspond to RNA (or the complex) and PTMD, respectively.

described HPLC-UV to quantify *Ka* values between DNA and low molecular weight compounds.[56−58]

Optimization by DOE. Design of experiments is a powerful statistical tool to select the method with the best chromatographic separation performance. Unlike the traditional one factor at a time (OFAT) approach, which adjusts a single parameter until the highest response is reached, the DOE allows the simultaneous optimization of multiple factors. Additionally, because multiple factors are varied at the same time, DOE can assess the interactions between them, providing a more comprehensive optimization strategy. In this study, we applied a DOE to optimize the migration time of RNA $[CUG]_{95}$, reducing the analysis time while maintaining a high selectivity between RNA and PTMD. The mobile phase consisted of aqueous 50 mM HEPES buffer at pH 7.4 and acetonitrile. The influence of three factors on the two

https://doi.org/10.1021/acsomega.5c09840
ACS Omega 2025, 10, 62205−62215

responses (migration time of RNA and selectivity) was studied: *(i)* the duration of the isocratic phase (100% aqueous phase) before starting the gradient (A), *(ii)* the gradient duration to reach 100% of the organic phase (B), and (iii) the flow rate of the mobile phase (C). The number of factors analyzed was low (3); therefore, the screening step, usually performed to highlight the most important ones, was bypassed, and the optimization was directly carried out. RSM (response surface methodology) was used with a CCD (central composite design), and a quadratic model was chosen since it showed the best determination coefficient value (0.9995). The factors of the model showing the highest desirability (0.988) were 1 min for A, 3.56 min for B, and 0.2 mL/min for C. The predicted responses using these conditions were 4.38 min and 1.25 for the retention time of RNA (Figure 8A) and the selectivity (Figure 8B), respectively. The experimental values obtained when performing the analysis were 4.35 min and 1.27, which were close to those predicted by the model.

Quantification of Apparent Affinity Constants. The optimized UPLC-UV method was therefore used to assess apparent affinity constants between PTMD and both $[CUG]_{95}$ and $[CUG]_{14}$ by analyzing several samples containing different concentrations of PTMD (Figure 9A,C).

Interactions were quantified using the Benesi−Hildebrand equation[56−58]

$$\frac{A_0}{(A - A_0)} = \frac{\epsilon_{RNA}}{\epsilon_C - \epsilon_{RNA}} + \frac{\epsilon_{RNA}}{\epsilon_C - \epsilon_{RNA}} \times \frac{1}{K_a \times [PTMD]} \quad (6)$$

In eq 6, A_0 is the peak area of RNA without PTMD, A is the peak area of RNA when PTMD is added, Ka is the affinity constant, [PTMD] is the concentration of PTMD, and ε_C and ε_{RNA} are the molar extinction coefficients of the complex RNA-PTMD and RNA, respectively. A linear regression was constructed by plotting $\frac{A_0}{(A-A_0)}$ as a function of $\frac{1}{[PTMD]}$ to to determine $Ka = \frac{\text{intercept}}{\text{slope}}$. Since this mathematical model also assumes a 1:1 stoichiometry, the determined affinity constant for other stoichiometries corresponds to the apparent affinity constant (Ka_{app}). Experiments were performed by testing each concentration in triplicate for both $[CUG]_{95}$ and $[CUG]_{14}$. The Ka_{app} values were $(6.0 \pm 6.3) \times 10^3$ M^{-1} and $(4.2 \pm 3.5) \times 10^3$ M^{-1} for the positive (Figure 9B) and negative (Figure 9D) controls, respectively.

An ANOVA study was conducted to compare these results with those obtained by ACE. The *p*-values were calculated to be 0.84 for the pathological model and 0.61 for the nonpathological model, indicating that the differences between the values obtained with both methods were insignificant using a risk α of 5%. Moreover, the comparison of the fittings obtained from both instrumental methods revealed that the standard deviations on the *y*-axis values and standard errors on the Ka_{app} values were considerably larger using UPLC-UV. These discrepancies were likely due to procedural differences. In ACE, the process was fully automated, whereas in UPLC-UV, PTMD was manually added to the RNA, introducing potential handling variability. Although the incubation time of the RNA and PTMD mixtures was standardized, this manual addition could lead to a supplementary risk of mishandling. Another hypothesis that might explain these discrepancies is the stability of the complex: *(i)* its interaction with the stationary phase might lead to conformational changes affecting its stability, and *(ii)* the elution step performed with acetonitrile might also influence the interaction properties between $[CUG]_n$ and PTMD. All of these aspects might explain the tailing phenomenon observed for the PTMD peaks in the chromatograms (Figure 9A,C) due to the progressive release of PTMD from the complexes. Finally, another key difference between the two methods was the volume of reagents necessary to perform the experiments. In ACE, the injection volumes of the tested RNA were around 10 nL, while they were 10 μL in UPLC-UV, making ACE more efficient for high-cost reagent analyses.

CONCLUSION

To the best of our knowledge, this is the first time that an optimized and consolidated ACE method has been proven to be a valuable analytical tool for quantifying interactions toward RNA probes representative of Steinert's disease. This worthy instrumental tool displays a very high degree of repeatability for the registered migration times (RSD lower than the threshold value set at 0.5%). Having a highly repeatable MT is crucial when performing assays with ACE equipment. As raw data, they will ensure the quality of any further quantitative determination. On the other hand, ACE is fully automated and can evaluate dozens of compounds, making it a suitable technique for high-throughput drug discovery, with the notable advantage of requiring minimal analyte and ligand consumption. Among the different compounds analyzed in this study, chloroquine appeared to interact selectively with the pathological RNA probe since its Ka_{app} was higher and significantly different from that measured for the negative control. Therefore, it represents a noteworthy candidate that will undoubtedly need further evaluation to confirm its efficacy in this context. Finally, our results highlight the potential of ACE in studying a large variety of compounds and identifying new therapeutic candidates for DM1, including compounds structurally related to PTMD, thereby overcoming its drawbacks.

ASSOCIATED CONTENT

Supporting Information

The Supporting Information is available free of charge at https://pubs.acs.org/doi/10.1021/acsomega.5c09840.

Library of aqueous soluble compounds, library of aqueous nonsoluble compounds, electropherograms of $[CUG]_{95}$ with chloroquine and neomycin at high concentrations, electropherograms (n = 45) of $[CUG]_{95}$ with 1% DMSO in the BGE (PDF)

AUTHOR INFORMATION

Corresponding Author

Bertrand Blankert − *Laboratory of Pharmaceutical Analysis, Faculty of Medicine Pharmacy and Biomedical Sciences, Health Research Institute, University of Mons, 7000 Mons, Belgium;* orcid.org/0000-0002-6667-7677; Email: Bertrand.blankert@umons.ac.be

Authors

Mathieu Leveque − *Laboratory of Pharmaceutical Analysis, Faculty of Medicine Pharmacy and Biomedical Sciences, Health Research Institute, University of Mons, 7000 Mons, Belgium*

Mathilde Wells − *Laboratory of Pharmaceutical Analysis, Faculty of Medicine Pharmacy and Biomedical Sciences, Health Research Institute, University of Mons, 7000 Mons, Belgium*
Delphine Beukens − *Laboratory of Pharmaceutical Analysis, Faculty of Medicine Pharmacy and Biomedical Sciences, Health Research Institute, University of Mons, 7000 Mons, Belgium*
Victor Lefebvre − *Laboratory of Pharmaceutical Analysis, Faculty of Medicine Pharmacy and Biomedical Sciences, Health Research Institute, University of Mons, 7000 Mons, Belgium*
Stéphanie Hambye − *Laboratory of Pharmaceutical Analysis, Faculty of Medicine Pharmacy and Biomedical Sciences, Health Research Institute, University of Mons, 7000 Mons, Belgium*

Complete contact information is available at: https://pubs.acs.org/10.1021/acsomega.5c09840

Author Contributions

M.L. developed and optimized the protocols, carried out the experiments, analyzed the data sets, and wrote the manuscript. D.B. and V.L. helped with the synthesis of biological materials. M.W., S.H., and B.B. supervised the research work. M.L., M.W., S.H., and B.B. contributed to the editing of the manuscript.

Funding

This research work was supported by a financial grant from the Association Belge contre les Maladies neuro-Musculaires (ABMM) and FNRS (Fonds de la Recherche Scientifique (projet FRSM No. 3.4614.11))

Notes

The authors declare no competing financial interest.

■ ACKNOWLEDGMENTS

We kindly thank the platform STATforU-UMONS (https://statforu.github.io/) for their efficient contribution.

■ REFERENCES

(1) Swinnen, B.; Robberecht, W.; Van Den Bosch, L. RNA toxicity in non-coding repeat expansion disorders. *EMBO J.* **2020**, *39*, No. e101112.
(2) Steinert, H. Myopathologische Beiträge. *Dtsch. Z. Nervenheilkd.* **1909**, *37*, 58−104.
(3) Fu, Y. H.; Pizzuti, A.; Fenwick, R. G.; et al. An unstable triplet repeat in a gene related to myotonic muscular dystrophy. *Science* **1992**, *255*, 1256−1258.
(4) Mahadevan, M.; Tsilfidis, C.; Sabourin, L.; et al. Myotonic dystrophy mutation: an unstable CTG repeat in the 3′ untranslated region of the gene. *Science* **1992**, *255*, 1253−1255.
(5) Napierala, M.; Krzyzosiak, W. J. CUG Repeats Present in Myotonin Kinase RNA Form Metastable "Slippery" Hairpins. *J. Biol. Chem.* **1997**, *272*, 31079−31085.
(6) LoRusso, S.; Weiner, B.; Arnold, W. D. Myotonic Dystrophies: Targeting Therapies for Multisystem Disease. *Neurotherapeutics* **2018**, *15*, 872−884.
(7) Taneja, K. L.; McCurrach, M.; Schalling, M.; Housman, D.; Singer, R. H. Foci of trinucleotide repeat transcripts in nuclei of myotonic dystrophy cells and tissues. *J. Cell Biol.* **1995**, *128*, 995−1002.
(8) Timchenko, L. T.; Timchenko, N. A.; Caskey, C. T.; Roberts, R. Novel proteins with binding specificity for DNA CTG repeats and RNA CUG repeats: implications for myotonic dystrophy. *Hum. Mol. Genet.* **1996**, *5*, 115−121.
(9) Miller, J. W.; et al. Recruitment of human muscleblind proteins to (CUG)(n) expansions associated with myotonic dystrophy. *EMBO J.* **2000**, *19*, 4439−4448.
(10) Mankodi, A.; et al. Muscleblind localizes to nuclear foci of aberrant RNA in myotonic dystrophy types 1 and 2. *Hum. Mol. Genet.* **2001**, *10*, 2165−2170.
(11) Fardaei, M.; Larkin, K.; Brook, J. D.; Hamshere, M. G. In vivo co-localisation of MBNL protein with DMPK expanded-repeat transcripts. *Nucleic Acids Res.* **2001**, *29*, 2766−2771.
(12) Kuyumcu-Martinez, N. M.; Wang, G.-S.; Cooper, T. A. Increased steady-state levels of CUGBP1 in myotonic dystrophy 1 are due to PKC-mediated hyperphosphorylation. *Mol. Cell* **2007**, *28*, 68−78.
(13) Jones, K.; Wei, C.; Iakova, P.; et al. GSK3β mediates muscle pathology in myotonic dystrophy. *J. Clin. Invest.* **2012**, *122*, 4461−4472.
(14) Wang, M.; Weng, W. C.; Stock, L.; et al. Correction of Glycogen Synthase Kinase 3β in Myotonic Dystrophy 1 Reduces the Mutant RNA and Improves Postnatal Survival of DMSXL Mice. *Mol. Cell. Biol.* **2019**, *39*, No. e00155-19, DOI: 10.1128/MCB.00155-19.
(15) López-Martínez, A.; Soblechero-Martín, P.; de-la-Puente-Ovejero, L.; Nogales-Gadea, G.; Arechavala-Gomeza, V. An Overview of Alternative Splicing Defects Implicated in Myotonic Dystrophy Type I. *Genes* **2020**, *11*, No. 1109, DOI: 10.3390/genes11091109.
(16) Johnson, N. E. Myotonic Muscular Dystrophies. *Continuum* **2019**, *25*, 1682−1695.
(17) Liao, Q.; Zhang, Y.; He, J.; Huang, K. Global Prevalence of Myotonic Dystrophy: An Updated Systematic Review and Meta-Analysis. *Neuroepidemiology* **2022**, *56*, 163−173.
(18) Johnson, N. E.; Butterfield, R. J.; Mayne, K.; et al. Population-Based Prevalence of Myotonic Dystrophy Type 1 Using Genetic Analysis of Statewide Blood Screening Program. *Neurology* **2021**, *96*, e1045−e1053.
(19) Izzo, M.; Battistini, J.; Provenzano, C.; et al. Molecular Therapies for Myotonic Dystrophy Type 1: From Small Drugs to Gene Editing. *Int. J. Mol. Sci.* **2022**, *23*, 4622.
(20) Timchenko, L. Development of Therapeutic Approaches for Myotonic Dystrophies Type 1 and Type 2. *Int. J. Mol. Sci.* **2022**, *23*, No. 10491.
(21) Warf, M. B.; Nakamori, M.; Matthys, C. M.; Thornton, C. A.; Berglund, J. A. Pentamidine reverses the splicing defects associated with myotonic dystrophy. *Proc. Natl. Acad. Sci. U.S.A.* **2009**, *106*, 18551−18556.
(22) Parkesh, R.; Childs-Disney, J. L.; Nakamori, M.; et al. Design of a Bioactive Small Molecule That Targets the Myotonic Dystrophy Type 1 RNA via an RNA Motif−Ligand Database and Chemical Similarity Searching. *J. Am. Chem. Soc.* **2012**, *134*, 4731−4742.
(23) Coonrod, L. A.; Nakamori, M.; Wang, W.; et al. Reducing levels of toxic RNA with small molecules. *ACS Chem. Biol.* **2013**, *8*, 2528−2537.
(24) Siboni, R. B.; Bodner, M. J.; Khalifa, M. M.; et al. Biological Efficacy and Toxicity of Diamidines in Myotonic Dystrophy Type 1 Models. *J. Med. Chem.* **2015**, *58*, 5770−5780.
(25) González, A. L.; Konieczny, P.; Llamusi, B.; et al. In silico discovery of substituted pyrido[2,3-d]pyrimidines and pentamidine-like compounds with biological activity in myotonic dystrophy models. *PLoS One* **2017**, *12*, No. e0178931.
(26) Neaga, I. O.; Hambye, S.; Bodoki, E.; et al. Affinity capillary electrophoresis for identification of active drug candidates in myotonic dystrophy type 1. *Anal. Bioanal. Chem.* **2018**, *410*, 4495−4507.
(27) Baroni, A.; Neaga, I.; Delbosc, N.; et al. Bioactive Aliphatic Polycarbonates Carrying Guanidinium Functions: An Innovative Approach for Myotonic Dystrophy Type 1 Therapy. *ACS Omega* **2019**, *4*, 18126−18135.

(28) Farcaş, E.; Pochet, L.; Crommen, J.; Servais, A.-C.; Fillet, M. Capillary electrophoresis in the context of drug discovery. *J. Pharm. Biomed. Anal.* **2017**, *144*, 195−212.
(29) Jing, M.; Bowser, M. T. Methods for measuring aptamer-protein equilibria: a review. *Anal. Chim. Acta* **2011**, *686*, 9−18.
(30) Thevendran, R.; Citartan, M. Assays to Estimate the Binding Affinity of Aptamers. *Talanta* **2022**, *238*, 122971.
(31) Neaga, I. O.; Bodoki, E.; Hambye, S.; Blankert, B.; Oprean, R. Study of nucleic acid−ligand interactions by capillary electrophoretic techniques: A review. *Talanta* **2016**, *148*, 247−256.
(32) Chu, Y. H.; Avila, L. Z.; Biebuyck, H. A.; Whitesides, G. M. Use of affinity capillary electrophoresis to measure binding constants of ligands to proteins. *J. Med. Chem.* **1992**, *35*, 2915−2917.
(33) Tanaka, Y.; Terabe, S. Estimation of binding constants by capillary electrophoresis. *J. Chromatogr., B Analyt. Technol. Biomed. Life. Sci.* **2002**, *768*, 81−92.
(34) Rundlett, K. L.; Armstrong, D. W. Methods for the determination of binding constants by capillary electrophoresis. *Electrophoresis* **2001**, *22*, 1419−1427.
(35) El-Hady, D.; Kühne, S.; El-Maali, N.; Wätzig, H. Precision in affinity capillary electrophoresis for drug-protein binding studies. *J. Pharm. Biomed. Anal.* **2010**, *52*, 232−241.
(36) Šolínová, V.; Mikysková, H.; Kaiser, M. M.; et al. Estimation of apparent binding constant of complexes of selected acyclic nucleoside phosphonates with β-cyclodextrin by affinity capillary electrophoresis. *Electrophoresis* **2016**, *37*, 239−247.
(37) Busch, M. H.; Carels, L. B.; Boelens, H. F.; Kraak, J. C.; Poppe, H. Comparison of five methods for the study of drug-protein binding in affinity capillary electrophoresis. *J. Chromatogr., A* **1997**, *777*, 311−328.
(38) Nowak, P. M.; Woźniakiewicz, M.; Gładysz, M.; Janus, M.; Kościelniak, P. Improving repeatability of capillary electrophoresis—a critical comparison of ten different capillary inner surfaces and three criteria of peak identification. *Anal. Bioanal. Chem.* **2017**, *409*, 4383−4393.
(39) Iki, N.; Yeung, E. S. Non-bonded poly(ethylene oxide) polymer-coated column for protein separation by capillary electrophoresis. *J. Chromatogr., A* **1996**, *731*, 273−282.
(40) Tran, N. T.; Taverna, M.; Miccoli, L.; Angulo, J. F. Poly(ethylene oxide) facilitates the characterization of an affinity between strongly basic proteins with DNA by affinity capillary electrophoresis. *Electrophoresis* **2005**, *26*, 3105−3112.
(41) Alahmad, Y.; Tran, N. T.; Le Potier, I.; et al. A new CZE method for profiling human serum albumin and its related forms to assess the quality of biopharmaceuticals. *Electrophoresis* **2011**, *32*, 292−299.
(42) Marie, A.-L.; Przybylski, C.; Gonnet, F.; et al. Capillary zone electrophoresis and capillary electrophoresis-mass spectrometry for analyzing qualitative and quantitative variations in therapeutic albumin. *Anal. Chim. Acta* **2013**, *800*, 103−110.
(43) Farcaş, E.; Bouckaert, C.; Servais, A. C.; et al. Partial filling affinity capillary electrophoresis as a useful tool for fragment-based drug discovery: A proof of concept on thrombin. *Anal. Chim. Acta* **2017**, *984*, 211−222.
(44) Ryczek, M.; Pluta, M.; Błaszczyk, L.; Kiliszek, A. Overview of Methods for Large-Scale RNA Synthesis. *Appl. Sci.* **2022**, *12*, 1543.
(45) Stellwagen, N. C.; Gelfi, C.; Righetti, P. G. The free solution mobility of DNA. *Biopolymers* **1997**, *42*, 687−703.
(46) Rehman, S. U.; Sarwar, T.; Husain, M. A.; Ishqi, H. M.; Tabish, M. Studying non-covalent drug−DNA interactions. *Arch. Biochem. Biophys.* **2015**, *576*, 49−60.
(47) Forman, S.; Kás, J.; Fini, F.; Steinberg, M.; Ruml, T. The effect of different solvents on the ATP/ADP content and growth properties of HeLa cells. *J. Biochem. Mol. Toxicol.* **1999**, *13*, 11−15.
(48) Lee, J.; Vogt, C. E.; McBrairty, M.; Al-Hashimi, H. M. Influence of dimethylsulfoxide on RNA structure and ligand binding. *Anal. Chem.* **2013**, *85*, 9692−9698.
(49) Charak, S.; Shandilya, M.; Mehrotra, R. RNA targeting by an anthracycline drug: spectroscopic and in silico evaluation of epirubicin interaction with tRNA. *J. Biomol. Struct. Dyn.* **2020**, *38*, 1761−1771.
(50) Subastri, A.; Ramamurthy, C.; Suyavaran, A.; et al. Probing the interaction of troxerutin with transfer RNA by spectroscopic and molecular modeling. *J. Photochem. Photobiol., B* **2015**, *153*, 137−144.
(51) Khan, A. Y.; Suresh Kumar, G. Spectroscopic studies on the binding interaction of phenothiazinium dyes, azure A and azure B to double stranded RNA polynucleotides. *Spectrochim. Acta, Part A* **2016**, *152*, 417−425.
(52) Saha, B.; Kumar, G. S. Spectroscopic and calorimetric investigations on the binding of phenazinium dyes safranine-O and phenosafranine to double stranded RNA polynucleotides. *J. Photochem. Photobiol., B* **2016**, *161*, 129−140.
(53) Hassan, A.; Sedenho, G. C.; Vitale, P. A. M.; Oliviera, M. N.; Crespilho, F. N. On the Weak Binding and Spectroscopic Signature of SARS-CoV-2 nsp14 Interaction with RNA. *Chembiochem* **2021**, *22*, 3410.
(54) Krochtová, K.; Janovec, L.; Bogárová, V.; Halečková, A.; Kožurková, M. Interaction of 3,9-disubstituted acridine with single stranded poly(rA), double stranded poly(rAU) and triple stranded poly(rUAU): molecular docking − A spectroscopic tandem study. *Chem. Biol. Interact.* **2024**, *394*, No. 110965.
(55) Charak, S.; Srivastava, C. M.; Kumar, D.; et al. Beyond DNA interactions: Insights into idarubicin's binding dynamics with tRNA using spectroscopic and computational approaches. *J. Photochem. Photobiol., B* **2025**, *266*, No. 113147.
(56) Kapcak, E.; Kara, H. E. S. Evaluation of interaction between DNA and anticancer drug Temozolomide and its degradation product by HPLC. *Rev. Roum. Chim.* **2018**, *63*, 1023−1034.
(57) Dindar, Ç. K.; Erkmen, C.; Yıldırım, S.; Bozal-Palabiyik, B.; Uslu, B. Interaction of citalopram and escitalopram with calf Thymus DNA: A spectrofluorometric, voltammetric, and liquid chromatographic approach. *J. Pharm. Biomed. Anal.* **2021**, *195*, No. 113891.
(58) Kuzpınar, E.; Al Faysal, A.; Şenel, P.; Erdoğan, T.; Gölcü, A. Quantification of mirtazapine in tablets via DNA binding mechanism; development of a new HPLC method. *J. Chromatogr., B* **2024**, *1234*, No. 124019.

https://doi.org/10.1021/acsomega.5c09840
ACS Omega 2025, 10, 62205−62215